Dark-bright solitons and semirational rogue waves for the coupled Sasa-Satsuma equations

Lei Liu, Bo Tian,* Yu-Qiang Yuan, and Zhong Du
State Key Laboratory of Information Photonics and Optical Communications, and School of Science, Beijing University of Posts and Telecommunications, Beijing 100876, China

(Received 12 December 2017; published 31 May 2018)

In this paper, we investigate the coupled Sasa-Satsuma equations, which describe the simultaneous propagation of two ultrashort pulses in the birefringent or two-mode fiber with the third-order dispersion, self-steepening, and stimulated Raman scattering effects. Darboux-dressing transformation is applied to obtain the dark-bright soliton and semirational rogue-wave solutions. Dark-bright one solitons with the single-hump, double-hump, and even breather-like structures are presented. Interactions between the double-peak breather and different kinds of dark-bright solitons are studied. We show that the double-peak (or single-peak) rogue wave can coexist and interact with different kinds of dark-bright solitons. Coexistence of the solitons with different velocities and rogue waves is also found. Numerical stabilities of the dark-bright solitons and semirational rogue waves are exhibited. It is expected that those localized wave phenomena can be experimentally observed and have potential applications.

DOI: 10.1103/PhysRevE.97.052217

I. INTRODUCTION

The scalar nonlinear Schrödinger (NLS) equations in the focusing and defocusing regimes have been applied in such physical fields as nonlinear optics, plasma physics, hydrodynamics, and Bose-Einstein condensation [1–4]. Localized waves for the scalar NLS equations, including bright solitons, dark solitons, breathers, and rogue waves, have been studied through experimental realization and theoretical analysis [1,5–10]. Moreover, researchers have focused their attention on some coupled equations due to applications in the multimode or wavelength-division multiplexing fibers, as well as multicomponent Bose-Einstein condensates [1,11–14]. Coupled NLS equations have been theoretically shown to support some vector solitons, rogue waves, and semirational rogue waves, which have more complicated features than the localized waves for the scalar NLS equations [11–15]. Those investigations have been claimed to contribute to understanding and controlling the behaviors of nonlinear waves [13–15].

In the nonlinear optics, for the intensive and short light pulses with the widths less than 100 fs, in addition to the group velocity dispersion and self-phase modulation, several higher-order linear and nonlinear effects have been considered, including the third-order dispersion (TOD), self-steepening (SS), and stimulated Raman scattering (SRS) [1,16,17]. With the simultaneous propagation of two ultrashort pulses in the birefringent or two-mode fiber, the coupled Sasa-Satsuma equations, which are the integrable extensions of the coupled NLS equations with the effects of TOD, SS, and SRS, have been presented [18–23]:

$$iq_{1z}+\tfrac{1}{2}q_{1tt}+(|q_1|^2+|q_2|^2)q_1+i\epsilon[q_{1ttt}+6(|q_1|^2+|q_2|^2)q_{1t}+3q_1(|q_1|^2+|q_2|^2)_t]=0, \quad (1a)$$

$$iq_{2z}+\tfrac{1}{2}q_{2tt}+(|q_1|^2+|q_2|^2)q_2+i\epsilon[q_{2ttt}+6(|q_1|^2+|q_2|^2)q_{2t}+3q_2(|q_1|^2+|q_2|^2)_t]=0, \quad (1b)$$

where q_1 and q_2 are the complex envelope amplitudes of the two field components, the subscripts z and t are the partial derivatives with respect to the normalized distance along the direction of propagation and retarded time, respectively, and the real constant ϵ (>0) scales a real perturbation parameter. If $\epsilon=0$, Eqs. (1) can be reduced to the coupled NLS equations [11]. Painlevé integrability for Eqs. (1) has been demonstrated [18]. Lax pair and bright-bright single-hump solitons for Eqs. (1) have been studied [19]. Bright-dark single- and double-hump solitons for Eqs. (1) have been presented via the Hirota method [20]. Certain vector W-shaped solitons for Eqs. (1) have been investigated through the Darboux transformations [21]. Through the binary Darboux transformations, bright-bright breather-like and vector antidark solitons for Eqs. (1) have been obtained [22]. Interactions between the bright-bright two solitons for Eqs. (1) have been exhibited [23].

Because of the existence of the SRS effect, Eqs. (1) under $q_2=0$, or the scalar Sasa-Satsuma equation, have been shown to support the richer localized wave phenomena than those from the scalar NLS equation [24–30]. For example, in addition to the bright single-hump solitons, the scalar Sasa-Satsuma equation has been shown to admit the bright double-hump and breather-like solitons [24], antidark and W-shaped solitons [25], breathers in a nonzero background and rogue waves with one-peak and double-peak structures [26–28], bright soliton interactions with six different cases [29], and higher-order and semirational rogue waves [30].

However, to our knowledge, there is still some work to be studied for Eqs. (1) besides Refs. [18–23]. Do Eqs. (1) admit the dark-bright breather-like solitons?[1] Do rogue waves

*tian_bupt@163.com

[1]This is different from the Akhmediev breather and Kuznetsov-Ma soliton for the NLS equation [7,9]; the dark breather-like soliton

 ©2018 American Physical Society

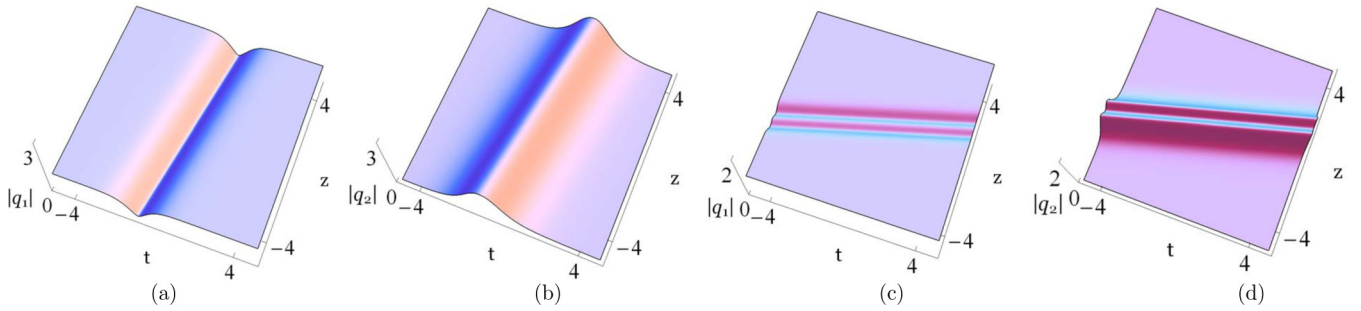

FIG. 1. Dark-bright one solitons via solutions (10), with $k = 1$, $\Gamma_4 = 0$, and $\Gamma_3 = 1$, (a) and (b) $\lambda_1 = 1.2 + 2.2i$ (single-hump); (c) and (d) $\lambda_1 = 0.2 + 1.6i$ (double-hump).

coexist with the double-hump even breather-like solitons for Eqs. (1)? Based on the above motivation, in this paper, we will investigate the dark-bright one soliton, soliton interactions, and semirational rogue waves for Eqs. (1) via the Darboux-dressing transformation [31–33]. In Sec. II, the first-iterated Darboux-dressing transformation formulas for Eqs. (1) will be given. We will respectively construct the dark-bright soliton and semirational rogue-wave solutions for Eqs. (1) through the two different vector solutions for the Lax pair. In Sec. III, by analyzing different parameters, we will find some abundant and complicated dark-bright soliton and semirational rogue wave features for Eqs. (1). In Sec. IV, numerical simulations will be used to investigate the dark-bright solitons and semirational rogue waves for Eqs. (1). Our summary and discussion will be presented in Sec. V.

II. DARK-BRIGHT SOLITON AND SEMIRATIONAL ROGUE-WAVE SOLUTIONS FOR EQS. (1)

By means of the Ablowitz-Kaup-Newell-Segur scheme [34], the Lax pair for Eqs. (1) can be obtained as

$$\Psi_t = U\Psi, \qquad \Psi_z = V\Psi, \tag{2}$$

where the vector eigenfunction $\Psi = (\psi_1, \psi_2, \psi_3, \psi_4, \psi_5)^T$, the superscript T signifies the transpose of a vector or matrix, ψ_ι ($\iota = 1,2,3,4,5$) are the complex functions of z and t, and the matrices U and V have the forms of

$$U = \lambda U_0 + U_1, \quad V = \lambda^3 V_0 + \lambda^2 V_1 + \lambda V_2 + V_3, \tag{3}$$

with

$$U_0 = \frac{i}{6\epsilon}\begin{pmatrix} -2 & \mathbf{0}^T \\ \mathbf{0} & I_4 \end{pmatrix}, \quad U_1 = \begin{pmatrix} 0 & Q \\ -Q^\dagger & \mathbf{O} \end{pmatrix},$$
$$Q = (-e^{-i\vartheta} q_1, -e^{i\vartheta} q_1^*, -e^{-i\vartheta} q_2, -e^{i\vartheta} q_2^*),$$
$$V_0 = \frac{1}{4\epsilon} U_0, \quad V_1 = \frac{1}{4\epsilon} U_1,$$
$$V_2 = -\frac{1}{12\epsilon} U_0 + \epsilon[U_{1t}, U_0] + \epsilon U_1 [U_1, U_0],$$
$$V_3 = -\frac{1}{12\epsilon} U_1 + \epsilon[U_{1t}, U_1] - \epsilon U_{1tt} + 2\epsilon U_1^3,$$

where $\vartheta = \frac{t}{6\epsilon} - \frac{z}{108\epsilon^2}$, $[X,Y] = XY - YX$ (both X and Y are the matrices), λ is the complex spectral parameter, I_4 is the 4×4 identity matrix, $\mathbf{O}$ is the 4×4 zero matrix, $\mathbf{0}$ is the 1×4 zero vector, $\dagger$ denotes the conjugate transpose, and $*$ means the complex conjugate. It can be verified that Eqs. (1) are equivalent to the compatibility condition $U_z - V_t + UV - VU = 0$.

Based on the analysis in Ref. [33], the first-iterated Darboux-dressing transformation formulas for Eqs. (1) are

has internal oscillations and multihump structures in a nonzero background, which characteristics correspond to the bright breather-like soliton [24].

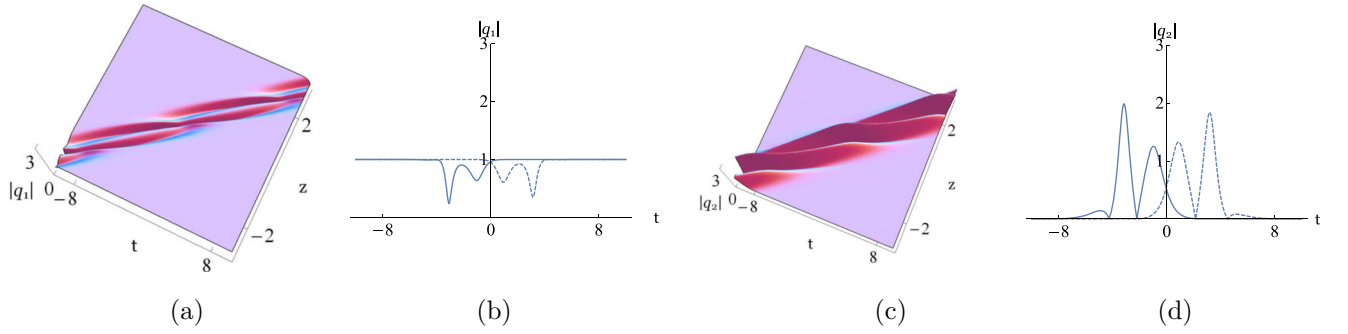

FIG. 2. Dark-bright breather-like one soliton via solutions (10), with $k = 1$, $\Gamma_3 = \Gamma_4 = 1$, and $\lambda_1 = 0.5 + 2.3i$. Panels (b) and (d) show corresponding trajectories of (a) and (c) at $z = -0.6$ (solid line) and $z = 0.6$ (dashed line), respectively.

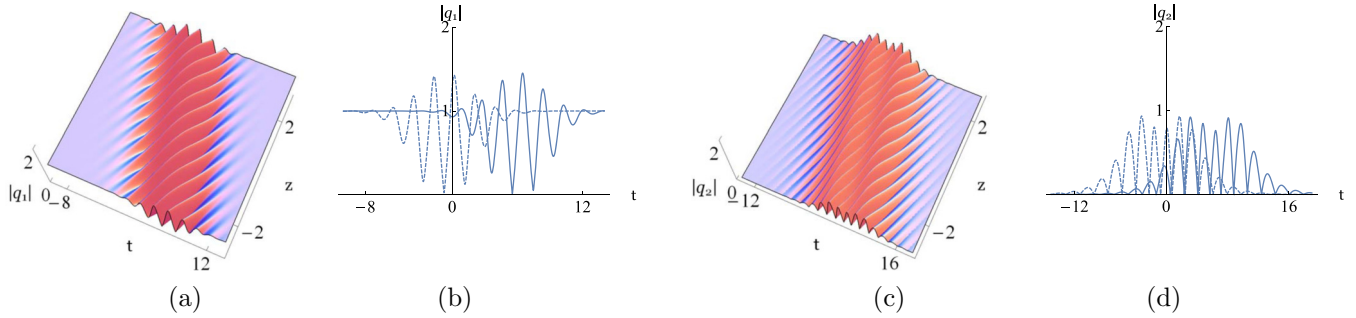

FIG. 3. Dark-bright breather-like one soliton via solutions (10), with the same parameters as in Fig. 2 except that $\lambda_1 = 0.3-1.8i$. Panels (b) and (d) show corresponding trajectories of (a) and (c) at $z = -3$ (solid line) and $z = 3$ (dashed line), respectively.

given as

$$q_1 = q_{1s} + \frac{i(\lambda_1 - \lambda_1^*)e^{i\vartheta}}{2\epsilon(\alpha^2 - |\beta|^2)}[(\alpha v_1 + \beta v_1^*)v_2^* + (\alpha v_1^* + \beta^* v_1)v_3], \tag{4a}$$

$$q_2 = q_{2s} + \frac{i(\lambda_1 - \lambda_1^*)e^{i\vartheta}}{2\epsilon(\alpha^2 - |\beta|^2)}[(\alpha v_1 + \beta v_1^*)v_4^* + (\alpha v_1^* + \beta^* v_1)v_5], \tag{4b}$$

where q_{1s} and q_{2s} denote the seed solutions for Eqs. (1), q_1 and q_2 denote the new solutions for Eqs. (1), λ_1 is a fixed value of the spectral parameter, the vector $(v_1, v_2, v_3, v_4, v_5)^T$ is the solution for Lax pair (2) with $\lambda = \lambda_1$, v_l are all the complex functions of z and t, and

$$\alpha = \sum_{\iota=1}^{5} |v_\iota|^2, \quad \beta = \frac{\lambda_1^* - \lambda_1}{2\lambda_1}\left(v_1^2 + 2v_2v_3 + 2v_4v_5\right).$$

To study the dark-bright soliton and semirational rogue wave, we choose the seed solutions as

$$q_{1s} = \frac{c}{2\epsilon}\exp\left[-\frac{i}{2\epsilon}\left(kt - \frac{\omega}{4\epsilon}z\right)\right], \quad q_{2s} = 0, \tag{5}$$

with

$$\omega = 2c^2K - k^2 - k^3,$$

where the amplitude parameter c and wave number k are both real constants, and $K \equiv 1 + 3k$. We need to notice that q_{1s} is in the nonzero background and q_{2s} is in the zero background. Then, for the different vector solution $(v_1, v_2, v_3, v_4, v_5)^T$, we have the results as follows. The details of the mathematical derivation are given in the Appendix.

(i) Solutions (4) are the dark-bright soliton solutions under

$$v_1 = e^{i\xi_1} + \Gamma_1 e^{i\xi_2} + \Gamma_2 e^{i\xi_3}, \tag{6a}$$

$$v_2 = \exp\left[i\vartheta + \frac{i}{2\epsilon}\left(kt - \frac{\omega}{4\epsilon}z\right)\right] \times (r_{11}e^{i\xi_1} + \Gamma_1 r_{12}e^{i\xi_2} + \Gamma_2 r_{13}e^{i\xi_3}), \tag{6b}$$

$$v_3 = \exp\left[-i\vartheta - \frac{i}{2\epsilon}\left(kt - \frac{\omega}{4\epsilon}z\right)\right] \times (r_{21}e^{i\xi_1} + \Gamma_1 r_{22}e^{i\xi_2} + \Gamma_2 r_{23}e^{i\xi_3}), \tag{6c}$$

$$v_4 = \Gamma_3 e^{i\xi_4}, \quad v_5 = \Gamma_4 e^{i\xi_4}, \tag{6d}$$

with

$$r_{jl} = \frac{-3ic}{m_l - (-1)^j K - \lambda_1}, \quad \xi_l = \frac{1}{6\epsilon}(m_l t + n_l z), \tag{7a}$$

$$n_l = -\frac{1}{36\epsilon}\left[3\lambda_1 m_l^2 + \left(3 + 36c^2 - K^2 - 6\lambda_1^2\right)m_l - 2\lambda_1\left(3\lambda_1^2 + 18c^2 + K^2\right)\right], \tag{7b}$$

$$\xi_4 = \frac{1}{6\epsilon}\left[\lambda_1 t + \frac{3\lambda_1^3 - \lambda_1}{12\epsilon}z\right], \quad j = 1,2, \quad l = 1,2,3, \tag{7c}$$

where m_l is defined in Eqs. (A9) of the Appendix and Γ_τ ($\tau = 1,2,3,4$) are all the complex constants. Note that here λ_1 is independent of k and c.

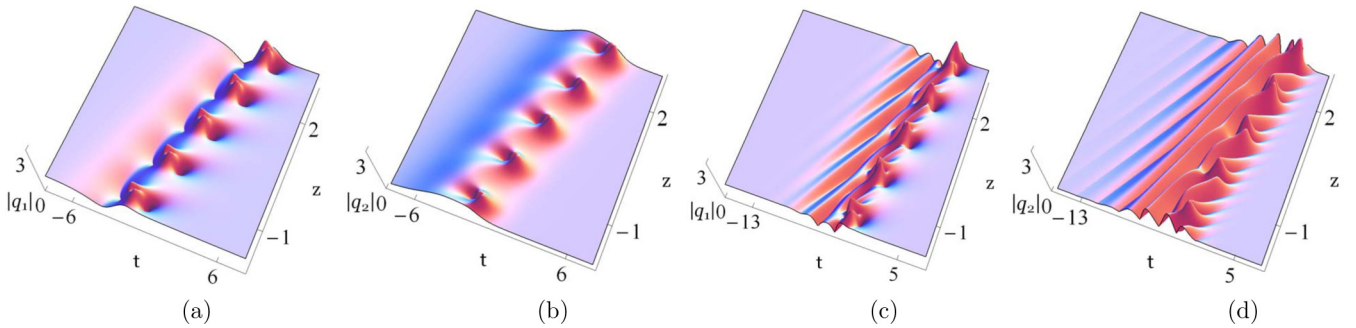

FIG. 4. Bound states between the breather and dark-bright soliton via Eqs. (4) and (6), with $\epsilon = 0.5$, $c = k = 1$, $\Gamma_2 = 0$, $\Gamma_1 = \Gamma_3 = 1$, and $\lambda_1 = 1.2 + 2.4102i$, (a) and (b) $\Gamma_4 = 0$ (single-hump soliton); (c) and (d) $\Gamma_4 = 1$ (breather-like soliton).

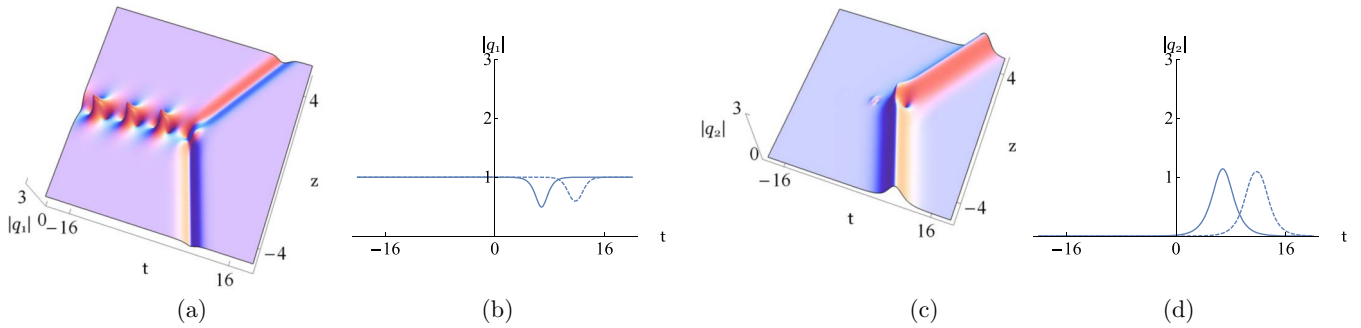

FIG. 5. Interaction between the breather and dark-bright soliton via Eqs. (4) and (6), with $\epsilon = 0.5$, $c = k = 1$, $\lambda_1 = 0.9 - 1.8i$, $\Gamma_1 = 1$, $\Gamma_3 = 0.5$ and $\Gamma_2 = \Gamma_4 = 0$. Panels (b) and (d) show corresponding trajectories of (a) and (c) at $z = -4$ (solid line) and $z = 4$ (dashed line), respectively.

(ii) Solutions (4) are the semirational rogue-wave solutions under

$$v_1 = e^{i\xi_1} + \Gamma_1 p_1 e^{i\xi_1} + \Gamma_2 e^{i\xi_3}, \tag{8a}$$

$$v_2 = \exp\left[i\vartheta + \frac{i}{2\epsilon}\left(kt - \frac{\omega}{4\epsilon}z\right)\right] \times (r_{11}e^{i\xi_1} + \Gamma_1 p_2 e^{i\xi_1} + \Gamma_2 r_{13} e^{i\xi_3}), \tag{8b}$$

$$v_3 = \exp\left[-i\vartheta - \frac{i}{2\epsilon}\left(kt - \frac{\omega}{4\epsilon}z\right)\right] \times (r_{21}e^{i\xi_1} + \Gamma_1 p_3 e^{i\xi_1} + \Gamma_2 r_{23} e^{i\xi_3}), \tag{8c}$$

$$v_4 = \Gamma_3 e^{i\xi_4}, \quad v_5 = \Gamma_4 e^{i\xi_4}, \tag{8d}$$

with

$$p_1 = \frac{i\mu}{216\epsilon^2}\left[36\epsilon t + \left(6\lambda_1^2 - 6\lambda_1 m_1 - 36c^2 + K^2 - 3\right)z\right], \tag{9a}$$

$$p_2 = \frac{c\mu\left[36\epsilon t + \left(6\lambda_1^2 - 6\lambda_1 m_1 - 36c^2 + K^2 - 3\right)z\right]}{72\epsilon^2(m_1 + K - \lambda_1)} + \frac{3ic\mu}{(m_1 + K - \lambda_1)^2}, \tag{9b}$$

$$p_3 = \frac{c\mu\left[36\epsilon t + \left(6\lambda_1^2 - 6\lambda_1 m_1 - 36c^2 + K^2 - 3\right)z\right]}{72\epsilon^2(m_1 - K - \lambda_1)} + \frac{3ic\mu}{(m_1 - K - \lambda_1)^2}, \tag{9c}$$

$$\lambda_1 = \pm\frac{i\sqrt{18c^2(9c^2 + 10K^2) - 4K^4 + 6c(9c^2 - 4K^2)^{3/2}}}{6K}, \tag{9d}$$

where ξ_τ and r_{jl} are defined in Eqs. (7), m_1 and m_3 are defined in Eqs. (A14) of the Appendix.

III. DARK-BRIGHT SOLITON AND SEMIRATIONAL ROGUE-WAVE PHENOMENA

Based on the analysis in Sec. II, we will discuss those soliton and rogue-wave phenomena, which are different from those in the coupled NLS equations [12–15]. In this section, without loss of generality, we keep parameters $\epsilon = 0.5$ and $c = 1$ in all discussion below, namely, the background remains constant 1.

For the dark-bright soliton and semirational rogue-wave solutions for Eqs. (1), it is noticed that in addition to the spectral parameter λ_1 and wave number k, the four complex constants Γ_1, Γ_2, Γ_3, and Γ_4 also play a role in the wave structures and nonlinear superpositions of waves. Hereby, we require that Γ_3 and Γ_4 are not both zero, or else $q_2 = 0$ and q_1 is reduced to a

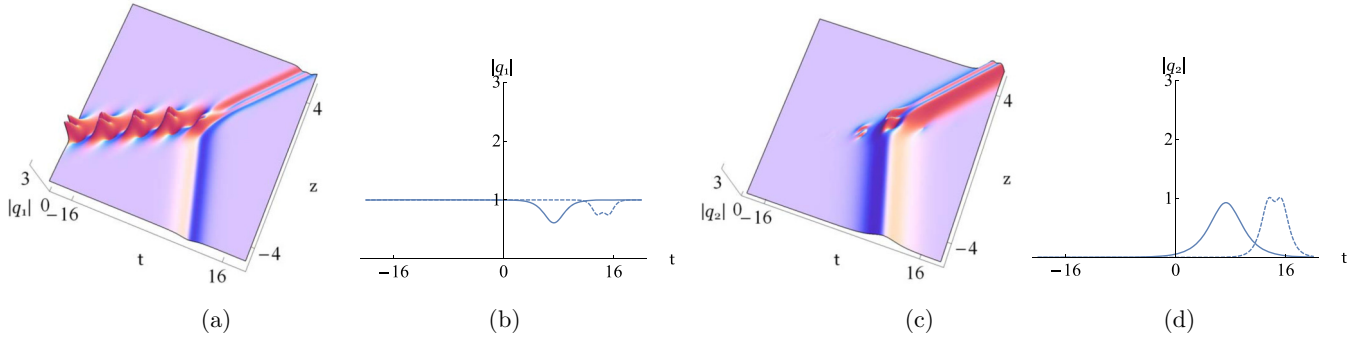

FIG. 6. Same as Fig. 5 except that $\lambda_1 = 0.4 - 1.8i$.

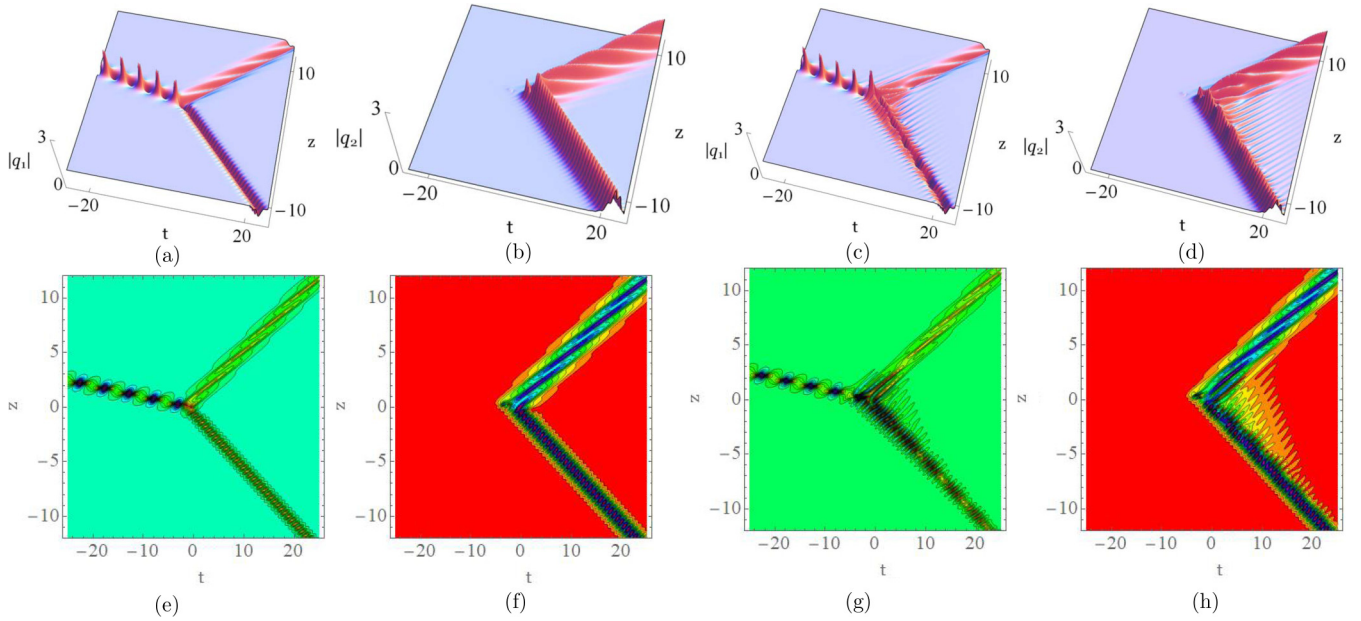

FIG. 7. Interactions between the breathers and dark-bright solitons via Eqs. (4) and (6), with $\epsilon = 0.5$, $c = k = 1$, $\lambda_1 = 1.2 - 1.8i$, $\Gamma_1 = \Gamma_3 = 1$, and $\Gamma_4 = 4$, (a) and (b) $\Gamma_2 = 0$; (c) and (d) $\Gamma_2 = 1$. Panels (e)–(h) show corresponding contour plots of (a)–(d), respectively.

solution of the scalar Sasa-Satsuma equation, which has been well studied in the previously reported [24–30].

A. Dark-bright solitons

Based on Eqs. (4) and (6), if setting $\Gamma_1 = \Gamma_2 = 0$, we can rewrite the dark-bright soliton solutions as

$$q_1 = \exp\left[-\frac{i}{2\epsilon}\left(kt - \frac{\omega}{4\epsilon}z\right)\right]\left[1 + i(\lambda_1 - \lambda_1^*)e^{i\vartheta}\frac{G_2}{G_1}\right],$$
$$q_2 = i(\lambda_1 - \lambda_1^*)e^{i\vartheta}\frac{G_3}{G_1}, \tag{10}$$

with

$$G_1 = 2|\lambda_1|^2\left[(|\Gamma_3|^2 + |\Gamma_4|^2) + e^{i(\xi_1-\xi_4)-i(\xi_1^*-\xi_4^*)} \times (1 + |r_{11}|^2 + |r_{21}|^2)\right]^2 + \tfrac{1}{2}(\lambda_1 - \lambda_1^*)^2 \times \left|2\Gamma_3\Gamma_4 + e^{2i(\xi_1-\xi_4)}(1 + 2r_{11}r_{21})\right|^2, \tag{11a}$$

$$G_2 = e^{2i(\xi_1-\xi_4)-2i(\xi_1^*-\xi_4^*)}h_1 + 2e^{i(\xi_1-\xi_4)-i(\xi_1^*-\xi_4^*)} \times (|\Gamma_3|^2 + |\Gamma_4|^2)|\lambda_1|^2(r_{11}^* + r_{21}) + 2(\lambda_1 - \lambda_1^*) \times \left[e^{2i(\xi_1-\xi_4)}\lambda_1\Gamma_3^*\Gamma_4^*r_{21} - e^{-2i(\xi_1^*-\xi_4^*)}\lambda_1^*\Gamma_3\Gamma_4 r_{11}^*\right], \tag{11b}$$

$$G_3 = \Gamma_3^*\lambda_1^* e^{2i(\xi_1-\xi_4)-i(\xi_1^*-\xi_4^*)}h_2 + \Gamma_4\lambda_1 e^{i(\xi_1-\xi_4)-2i(\xi_1^*-\xi_4^*)}h_2^* + 2\left[\Gamma_3^*\lambda_1 e^{i(\xi_1-\xi_4)} + \Gamma_4\lambda_1^* e^{-i(\xi_1^*-\xi_4^*)}\right] \times (|\Gamma_3|^2\lambda_1^* + |\Gamma_4|^2\lambda_1), \tag{11c}$$

$$h_1 = (\lambda_1 + \lambda_1^*)(\lambda_1 r_{21} + \lambda_1^* r_{11}^*) + 2(\lambda_1|r_{21}|^2 + \lambda_1^*|r_{11}|^2)(\lambda_1 r_{11}^* + \lambda_1^* r_{21}), \tag{11d}$$

$$h_2 = [1 + 2(|r_{11}|^2 - r_{11}r_{21} + |r_{21}|^2)]\lambda_1 + (1 + 2r_{11}r_{21})\lambda_1^*. \tag{11e}$$

From solutions (10) and (11), we know that the soliton velocities are measured by the relative factor $e^{i(\xi_1-\xi_4)-i(\xi_1^*-\xi_4^*)}$. We say that such solutions are the vector one-soliton solutions. The soliton velocities in the q_1 and q_2 components are the same

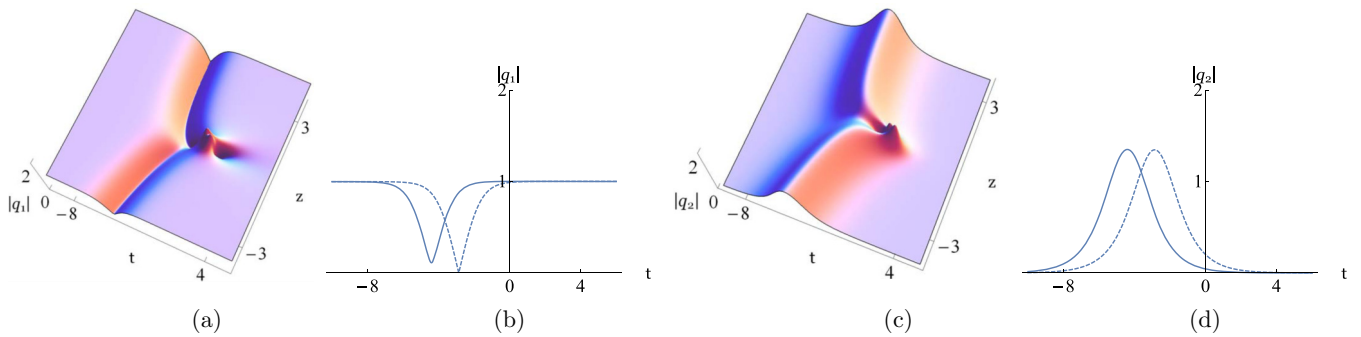

FIG. 8. Vector semirational rogue wave via solutions (13), with $\mu = 1$, $k = 1.2$, $\Gamma_1 = 4$, $\Gamma_3 = 1$, and $\Gamma_2 = \Gamma_4 = 0$. Panels (b) and (d) show corresponding trajectories of (a) and (c) at $z = -4$ (solid line) and $z = 4$ (dashed line), respectively.

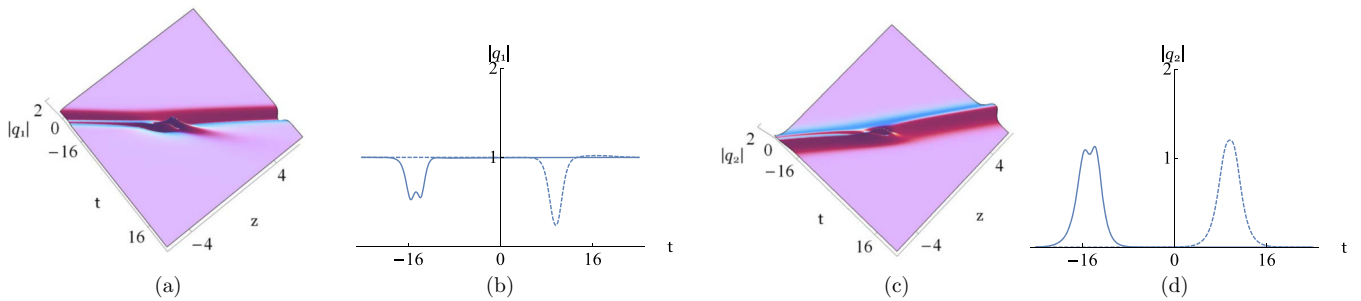

FIG. 9. Same as Fig. 8 except that $k = 0.35$.

and are expressed as

$$V_{s1} = \frac{39 - K^2}{18} + \frac{\lambda_1(m_1 - \lambda_1)^2 - \lambda_1^*(m_1^* - \lambda_1^*)^2 - K^2(\lambda_1 - \lambda_1^*)}{6[(m_1 - m_1^*) - (\lambda_1 - \lambda_1^*)]}, \tag{12}$$

where m_1 is defined in Eqs. (A9) by parameters λ_1 and K. Therefore, we can see that the velocity of the dark-bright soliton is related to spectral parameter λ_1 and wave number k. Besides, because the soliton solutions may exhibit multihump structures, the expressions of soliton average amplitudes are rather cumbersome and are not discussed in this paper. Even so, we can still see that the soliton amplitudes in the q_1 and q_2 components depend on all parameters λ_1, k, Γ_3, and Γ_4.

When $\Gamma_3 = 0$ (or $\Gamma_4 = 0$), we observe the dark-bright one soliton with single-hump or double-hump structure for Eqs. (1), as shown in Fig. 1. For the different spectral parameter λ_1, the dark-bright one soliton maybe exhibit one or two maximum amplitudes. In Ref. [20], those vector solitons have also been obtained through the Hirota method.

However, when $\Gamma_3\Gamma_4 \neq 0$, we observe two types of the dark-bright breather-like one soliton for different λ_1. In Fig. 2, the dark and bright contributions in the q_1 and q_2 components have internal oscillations and multihump structures. Although the scalar Sasa-Satsuma equation supports the bright breather-like soliton [24], the dark breather-like soliton is still difficult to be obtained for the scalar Sasa-Satsuma equation in both focusing and defocusing [35]. In Figs. 3, the q_1 component shows the superposition of the dark and bright contributions and gives rise to a breather-like soliton which is different from that in Fig. 2(a), and the q_2 component still exhibits multihump structures with oscillation. In fact, the coexistence of factors $e^{i(\xi_1-\xi_4)-i(\xi_1^*-\xi_4^*)}$ and $e^{2i(\xi_1-\xi_4)-2i(\xi_1^*-\xi_4^*)}$ in solutions (10) causes the intensities of $|q_1|$ and $|q_2|$ to possess possible double-hump structures, and on that basis, factors $e^{i(\xi_1-\xi_4)}$ and $e^{-i(\xi_1^*-\xi_4^*)}$ cause the intensities of $|q_1|$ and $|q_2|$ to possess some oscillating structures. Furthermore, the double-hump and multihump vector solitons have been said to have potential applications in the higher bit-rate transmission for multilevel communication [36,37].

On the other hand, from Eqs. (6), we can see that if Γ_1 or Γ_2 is not zero, there are more relative factors, such as $e^{i(\xi_2-\xi_4)-i(\xi_2^*-\xi_4^*)}$ and $e^{i(\xi_3-\xi_4)-i(\xi_3^*-\xi_4^*)}$. Therefore, the solutions will have more than one branch, that is, we can observe the interactions and coexistence phenomena between breathers and dark-bright solitons. Such solutions can be represented by Eqs. (4) and (6), but we will not present those due to the complication.

We consider $\Gamma_2 = 0$ and $\Gamma_1\Gamma_3 \neq 0$ in Eqs. (6). We assume that the breather and dark-bright soliton have the same velocity, that is, the parameters satisfy the following constraint:

$$\frac{\lambda_1(m_1 - \lambda_1)^2 - \lambda_1^*(m_1^* - \lambda_1^*)^2 - K^2(\lambda_1 - \lambda_1^*)}{(m_1 - m_1^*) - (\lambda_1 - \lambda_1^*)} = \frac{\lambda_1(m_2 - \lambda_1)^2 - \lambda_1^*(m_2^* - \lambda_1^*)^2 - K^2(\lambda_1 - \lambda_1^*)}{(m_2 - m_2^*) - (\lambda_1 - \lambda_1^*)}.$$

For this purpose, choosing $\lambda_1 \approx 1.2 + 2.4102i$ and $k = 1$ (i.e., $K = 4$), we obtain the bound states between the breather and

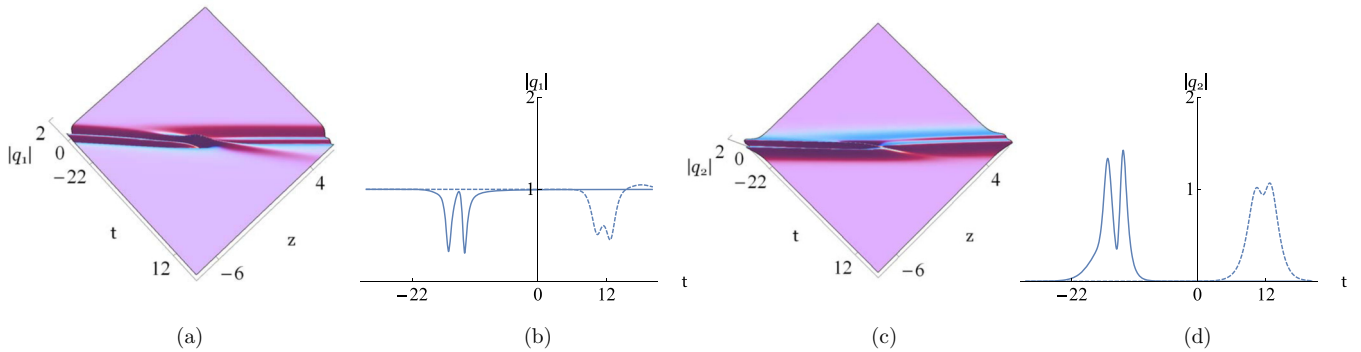

FIG. 10. Same as Fig. 8 except that $k = 0.19$.

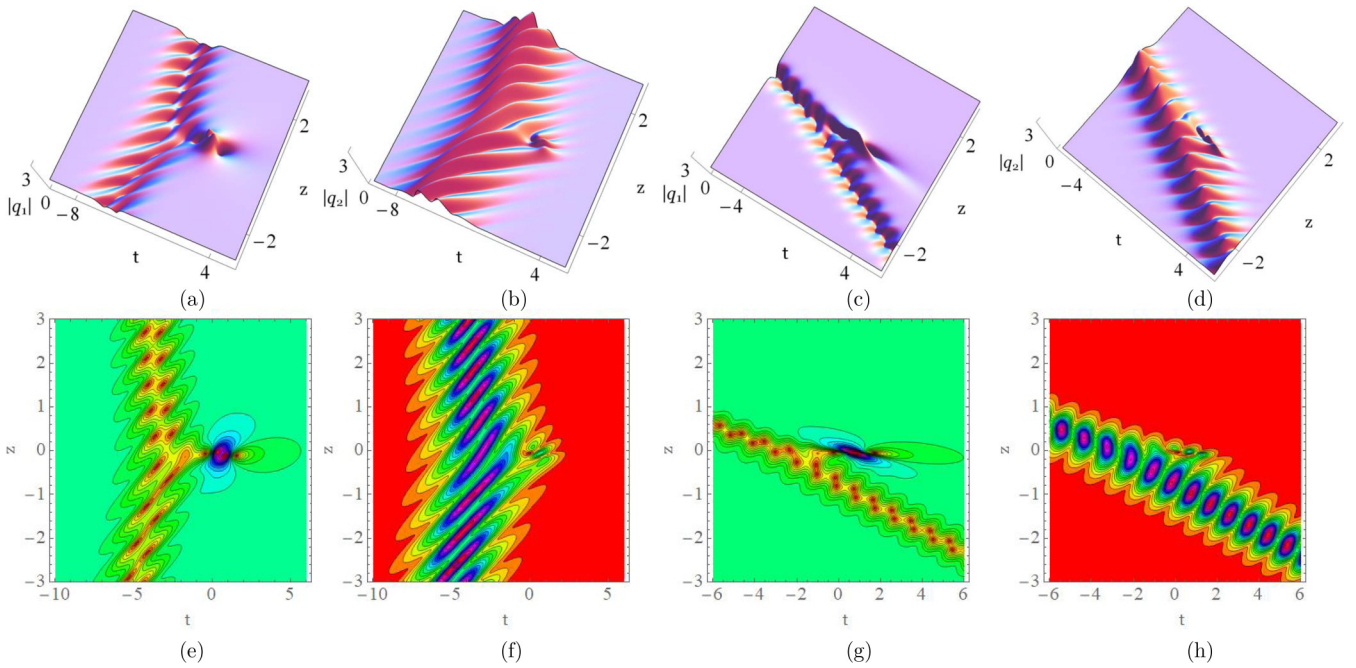

FIG. 11. Vector semirational rogue waves via solutions (13), with $\mu = 1$, $\Gamma_1 = 10$, $\Gamma_2 = 0$, $\Gamma_3 = 1$, and $\Gamma_4 = 0.5$, (a) and (b) $k = 1.2$; (c) and (d) $k = 2$. Panels (e)–(h) show corresponding contour plots of (a)–(d), respectively.

dark-bright soliton, as shown in Fig. 4. Under the constraint, the velocity of both the breather and dark-bright soliton is approximately 1.04. As seen in Figs. 4(a) and 4(b), when $\Gamma_4 = 0$, the breather with double-peak structure coexists with the dark-bright single-hump soliton. When $\Gamma_4 \neq 0$, the double-peak breather coexists with the dark-bright breather-like soliton, as seen in Figs. 4(c) and 4(d).

When the breathers and dark-bright solitons have different velocities, reflecting interactions between breathers and dark-bright solitons will occur. Instead of the asymptotic analysis, we show such behaviors in Figs. 5–7. If $\Gamma_4 = 0$, as seen in Figs. 5(a) and 5(b), the single-hump dark-bright soliton changes its velocity after the interaction with the double-peak breather. It seems that the dark-bright soliton is reflected when it interacts with the breather. In addition to the change of velocities, in Figs. 5(b) and 5(d), we see that the amplitudes of the single-hump soliton in the q_1 and q_2 components slightly decrease after such interaction. In Fig. 6, we see that the single-hump soliton converts into the double-hump soliton after the interaction. And both amplitudes and velocities of the soliton in the q_1 and q_2 components are changed after such interaction. However, when choosing $\Gamma_4 \neq 0$, we see that the dark-bright solitons possess some oscillating structures, as shown in Fig. 7. In particular, Figs. 7(c) and 7(d) exhibit the interaction under $\Gamma_2\Gamma_4 \neq 0$. To clearly show the effect of the parameter Γ_2, we use the corresponding contour plots in Figs. 7(e)–7(h). Compared with Figs. 7(a) and 7(b), Figs. 7(c) and 7(d) show more complicated oscillation before and after the interaction, while when $z \to \pm\infty$, such dark-bright solitons seem to be unaffected. Namely, the parameter Γ_2 does not affect the asymptotic behavior of the dark-bright soliton except for some oscillation in the interaction domains. Similar phenomena can also apply to the cases of Figs. 5 and 6. All of those reflecting interactions are inelastic.

B. Semirational rogue waves

Via Eqs. (4) and (8) and under $\Gamma_2 = 0$, the semirational rogue-wave solutions are rewritten as

$$q_1 = \exp\left[-\frac{i}{2\epsilon}\left(kt - \frac{\omega}{4\epsilon}z\right)\right]\left[1 + i(\lambda_1 - \lambda_1^*)e^{i\vartheta}\frac{F_2}{F_1}\right],$$
$$q_2 = i(\lambda_1 - \lambda_1^*)e^{i\vartheta}\frac{F_3}{F_1}, \tag{13}$$

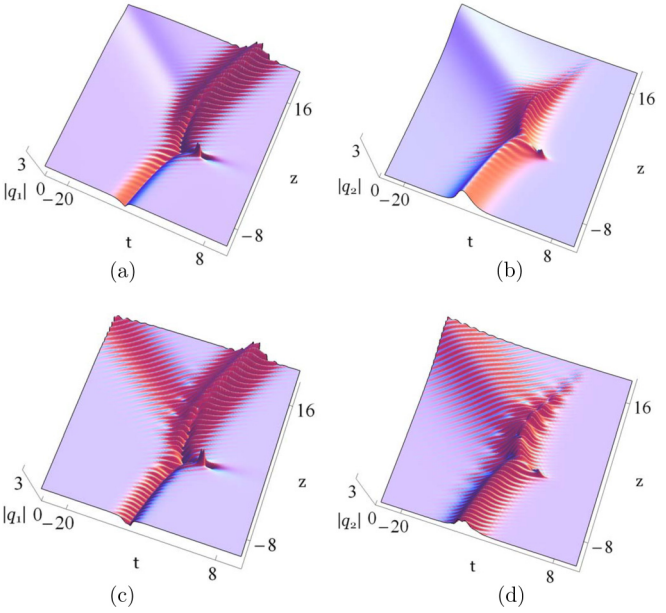

FIG. 12. Vector semirational rogue waves via Eqs. (4) and (8), with $\epsilon = 0.5$, $c = \mu = 1$, $k = 1.2$, $\Gamma_1 = 10$, $\Gamma_2 = 0.1$, and $\Gamma_3 = 1$, (a) and (b) $\Gamma_4 = 0$; (c) and (d) $\Gamma_4 = 0.5$.

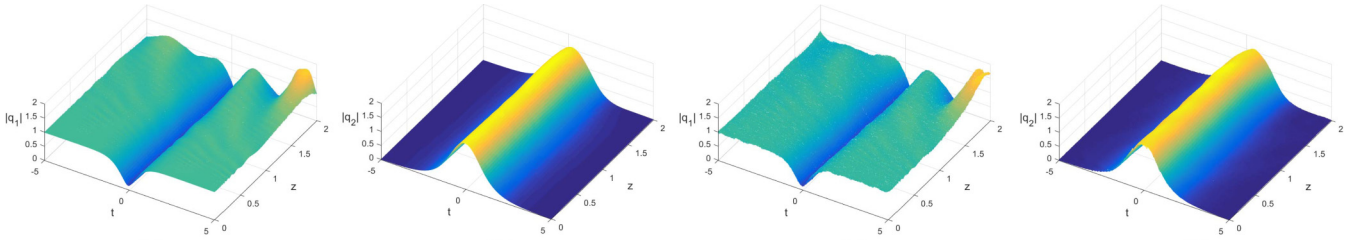

FIG. 13. Numerical simulations of the dark-bright soliton via solutions (10), with $k = 1$, $\Gamma_3 = 1$, $\Gamma_4 = 0$, and $\lambda_1 = 1.2 + 2.2i$. (a) and (b) the unperturbed initial pulses; (c) and (d) the perturbed initial pulses by white noise.

with

$$F_1 = 2|\lambda_1|^2\big[(|\Gamma_3|^2 + |\Gamma_4|^2) + e^{i(\xi_1-\xi_4)-i(\xi_1^*-\xi_4^*)}(1 + |r_{11}|^2 + |r_{21}|^2 + w_1)\big]^2$$
$$+ \tfrac{1}{2}(\lambda_1 - \lambda_1^*)^2|2\Gamma_3\Gamma_4 + e^{2i(\xi_1-\xi_4)}(1 + 2r_{11}r_{21} + w_2)|^2, \tag{14a}$$

$$F_2 = e^{2i(\xi_1-\xi_4)-2i(\xi_1^*-\xi_4^*)}w_3 + 2e^{i(\xi_1-\xi_4)-i(\xi_1^*-\xi_4^*)}(|\Gamma_3|^2 + |\Gamma_4|^2)|\lambda_1|^2w_4 + 2(\lambda_1 - \lambda_1^*)$$
$$\times \big[e^{2i(\xi_1-\xi_4)}\lambda_1\Gamma_3^*\Gamma_4^*(1 + \Gamma_1p_1)(r_{21} + \Gamma_1p_3) - e^{-2i(\xi_1^*-\xi_4^*)}\lambda_1^*\Gamma_3\Gamma_4(1 + \Gamma_1^*p_1^*)(r_{11}^* + \Gamma_1^*p_2^*)\big], \tag{14b}$$

$$F_3 = \Gamma_3^*\lambda_1^*e^{2i(\xi_1-\xi_4)-i(\xi_1^*-\xi_4^*)}w_5 + \Gamma_4\lambda_1e^{i(\xi_1-\xi_4)-2i(\xi_1^*-\xi_4^*)}w_5^*$$
$$+ 2\big[\Gamma_3^*\lambda_1(1 + \Gamma_1p_1)e^{i(\xi_1-\xi_4)} + \Gamma_4\lambda_1^*(1 + \Gamma_1^*p_1^*)e^{-i(\xi_1^*-\xi_4^*)}\big](|\Gamma_3|^2\lambda_1^* + |\Gamma_4|^2\lambda_1), \tag{14c}$$

$$w_1 = \Gamma_1(p_1 + p_2r_{11}^* + p_3r_{21}^*) + \Gamma_1^*(p_1^* + p_2^*r_{11} + p_3^*r_{21}) + |\Gamma_1|^2(|p_1|^2 + |p_2|^2 + |p_3|^2), \tag{14d}$$

$$w_2 = 2\Gamma_1(p_1 + p_3r_{11} + p_2r_{21}) + \Gamma_1^2\big(p_1^2 + 2p_2p_3\big), \tag{14e}$$

$$w_3 = |1 + \Gamma_1p_1|^2(\lambda_1 + \lambda_1^*)\big[\lambda_1(r_{21} + \Gamma_1p_3)(1 + \Gamma_1^*p_1^*) + \lambda_1^*(r_{11}^* + \Gamma_1^*p_2^*)(1 + \Gamma_1p_1)\big]$$
$$+ 2(\lambda_1|r_{21} + \Gamma_1p_3|^2 + \lambda_1^*|r_{11} + \Gamma_1p_2|^2)\big[\lambda_1(r_{11}^* + \Gamma_1^*p_2^*)(1 + \Gamma_1p_1) + \lambda_1^*(r_{21} + \Gamma_1p_3)(1 + \Gamma_1^*p_1^*)\big], \tag{14f}$$

$$w_4 = r_{11}^* + r_{21} + \Gamma_1(p_3 + p_1r_{11}^*) + \Gamma_1^*(p_2^* + p_1^*r_{21}) + |\Gamma_1|^2(p_1p_2^* + p_1^*p_3), \tag{14g}$$

$$w_5 = [1 + 2(|r_{11}|^2 - r_{11}r_{21} + |r_{21}|^2) + \Delta_1 + \Delta_2]\lambda_1 + (1 + 2r_{11}r_{21} + w_2)(1 + \Gamma_1^*p_1^*)\lambda_1^*, \tag{14h}$$

$$\Delta_1 = 2\Gamma_1p_1(|r_{11}|^2 + |r_{21}|^2) + \Gamma_1^*p_1^*(1 - 2r_{11}r_{21}) + \Gamma_1(1 + p_1^*\Gamma_1^*)\big[2p_1 - 2p_2r_{21} - 2p_3r_{11} + \Gamma_1\big(p_1^2 - 2p_2p_3\big)\big], \tag{14i}$$

$$\Delta_2 = 2(1 + p_1\Gamma_1)[\Gamma_1(p_2r_{11}^* + p_3r_{21}^*) + \Gamma_1^*(p_2^*r_{11} + p_3^*r_{21}) + |\Gamma_1|^2(|p_2|^2 + |p_3|^2)]. \tag{14j}$$

We can see that if $\Gamma_1 = 0$, solutions (13) are reduced to the dark-bright soliton solutions. Only if $\Gamma_1 \neq 0$, solutions (13) contain polynomial functions; that is, vector semirational rogue-wave solutions can be obtained. It is noted that λ_1 in solutions (13) is not a free parameter, but is determined by Eq. (A15), which is different from solutions (10).

Semirational rogue-wave solutions (13) show that the rogue wave coexists and interacts with dark-bright soliton. When $\Gamma_4 = 0$ (or $\Gamma_3 = 0$), based on the analysis of the relative exponential factors, we know that the dark-bright soliton constituents only appear with single-hump or double-hump structures. When we change the parameter k (here λ_1 is also changed), several different interactions will be generated.

For example, when $k = 1.2$, Figs. 8(a) and 8(c) show a single-hump dark-bright soliton together with a double-peak rogue wave. As seen in Figs. 8(b) and 8(d), the soliton amplitudes in the q_1 and q_2 components are changed during such interaction [in Fig. 8(d), the amplitude also changes slightly]. Decreasing the value of k, we see that the double-hump dark-bright soliton converts into to the single-hump dark-bright soliton after the interaction with a double-peak rogue wave, as shown in Fig. 9. When $k = 0.19$, Fig. 10 shows a double-hump dark-bright soliton coexisting with a single-peak rogue wave. We can see that the rogue wave and dark-bright solitons almost merge together. From the trajectories in Figs. 9 and 10, we see that the dark-bright solitons change their shapes during the interaction with the rogue waves. In such interaction domains, there are obvious changes for the velocities of solitons. With the decrease of k, the velocities of solitons in the asymptotic behaviors gradually become larger along the positive direction [the velocity expression of the soliton is the same as Eq. (12) despite the difference of λ_1 and m_1]. It is noted that the double-hump solitons in Figs. 9 and 10 are not symmetric for the smaller $|z|$ due to the effect of interactions. However,

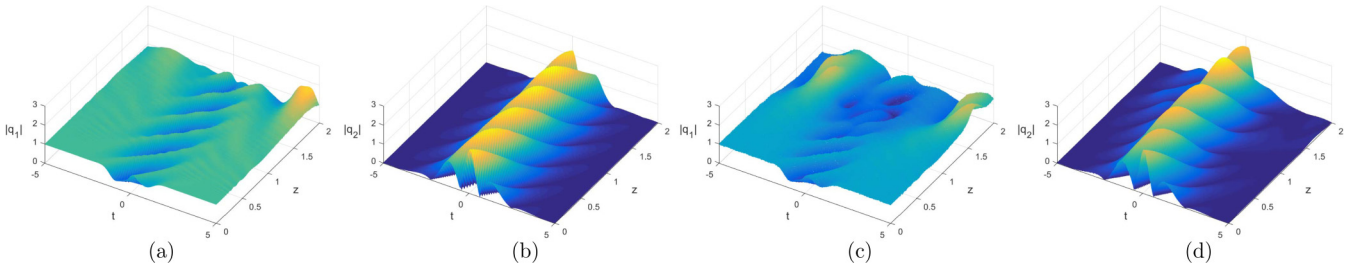

FIG. 14. Same as Fig. 13 except that $\Gamma_4 = 1$.

when the value of $|z|$ becomes larger, such solitons will present symmetric double-hump structures.

Similarly, when $\Gamma_3\Gamma_4 \neq 0$, factors $e^{i(\xi_1-\xi_4)}$ and $e^{-i(\xi_1^*-\xi_4^*)}$ in solutions (13) cause the dark-bright soliton constituents to possess some oscillating structures. As shown in Fig. 11, we observe that the rogue waves coexist and interact with the dark-bright breather-like solitons. Because the component q_2 is in zero background, those phenomena are different from the vector breather solitons in the coupled NLS equations [13]. When $k = 1.2$, the rogue wave exhibits a double-peak structure, and the velocity of the soliton for the larger $|z|$ is approximately 0, as shown in Figs. 11(a) and 11(b). Increasing the value of k, we find that the rogue wave changes its structure to a single peak, and the velocity of the soliton for the lager $|z|$ is changed to a negative value, as shown in Figs. 11(c) and 11(d). From Figs. 11(e)–11(h), we see that the interactions also change the shapes of the dark-bright solitons.

Finally, we consider a complicated case, i.e., $\Gamma_2 \neq 0$. Under this case, a nonlinear superposition of solitons with different velocities and a rogue wave will occur. Because of the complication of the solutions, we just discuss the properties via the graphical analysis. In Fig. 12, we observe that the dark-bright solitons and rogue waves coexist. When $\Gamma_4 = 0$, we see that a dark-bright single-hump soliton diverges into another dark-bright single-hump soliton and a breather-like soliton after the interaction with the double-peak rogue wave, as shown in Figs. 11(a) and 11(b). When $\Gamma_4 \neq 0$, all dark-bright soliton constituents exhibit the breather-like structures, as seen in Figs. 11(c) and 11(d). Additionally, in Fig. 11, some oscillations always appear near the rogue waves in the q_1 and q_2 components, whether $\Gamma_4 = 0$ or $\Gamma_4 \neq 0$.

IV. NUMERICAL SIMULATIONS

In this section, we use numerical simulations to investigate the stability of the dark-bright soliton and semirational rogue-wave solutions. Here, we used a split-step Fourier method to solve the linear part and a fourth-order Runge-Kutta method to deal with the nonlinear part for Eqs. (1). With or without exerting white noise perturbation, numerical results of the dark-bright soliton and semirational rogue-wave solutions are demonstrated in Figs. 13–16. Here, we mimic the initial pulses perturbed with 5% white noise of small amplitudes. Namely, we multiply the q_1 and q_2 by the factors $[1 + 0.05 f_j(t)]$ $(j = 1,2)$, respectively, where $f_j(t)$ are uncorrelated random functions uniformly distributed in the interval $[-1,1]$.

We choose the initial pulse inputs via solutions (10) at $z = 0$. The initial pulse parameters in Fig. 13 are the same as those in Figs. 1(a) and 1(b). We see that the unperturbed numerical solutions in Figs. 13 and 14 reproduce the dark-bright solitons with the single-hump and breather-like structures, which agree with the analytical solutions of dark-bright soliton for Eqs. (1). Due to the fact that the modulation instability tends to interfere strongly with the trailing edge of the localized solutions [14], the unstable backgrounds when $z > 1.6$ are presented for the dark components in Figs. 13 and 14. Under the white noise perturbation, Figs. 13(c) and 13(d) present the stability of the dark-bright soliton with the single-hump structure. In Figs. 14(c) and 14(d), the dark component of the dark-bright soliton with the breather-like structure exhibits instability, while the bright one seems to be stable.

Then, we consider solutions (13) at $z = -1$ as the initial pulses. The initial pulse parameters in Fig. 15 are the same as those in Fig. 8. The unperturbed numerical solutions in Figs. 15 and 16 reproduce the coexistence of the double-peak rogue wave and dark-bright solitons with the single-hump and breather-like structures, which agree with the analytical solutions of the semirational rogue waves for Eqs. (1). Similarly, for the q_1 component, we see that the modulation instability tends to interfere strongly with the trailing edge of the localized solutions when $z > 1$. Under the white noise perturbation of the semirational rogue waves, Figs. 15 and 16 reveal that the

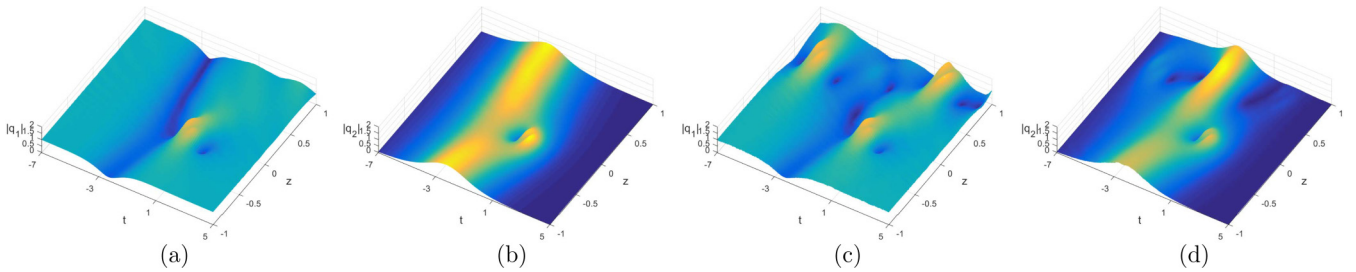

FIG. 15. Numerical simulations of the semirational rogue wave via solutions (13), with $\mu = 1$, $k = 1.2$, $\Gamma_1 = 4$, $\Gamma_3 = 1$, and $\Gamma_4 = 0$. (a) and (b) the unperturbed initial pulses; (c) and (d) the perturbed initial pulses by white noise.

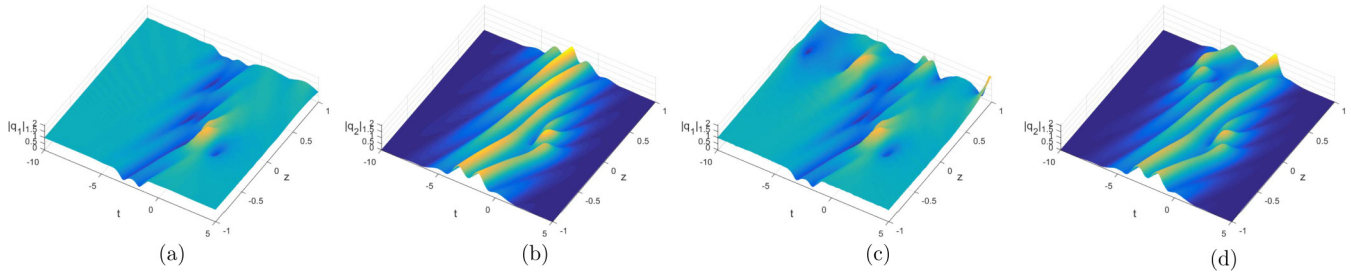

FIG. 16. Same as Figs. 15 except that $\Gamma_4 = 0.5$.

double-peak rogue wave constituents seem to be stable on an unstable background, while the dark-bright soliton constituents exhibit instability.

V. SUMMARY AND DISCUSSION

In summary, we have studied the coupled Sasa-Satsuma equations, i.e., Eqs. (1), which describe the simultaneous propagation of two ultrashort pulses in the birefringent or two-mode fiber with the TOD, SS, and SRS effects. Based on Lax pair (2), we have respectively derived two different vector solutions, i.e., solutions (6) and (8). With the help of the first-iterated Darboux-dressing transformation formulas, i.e., Eqs. (4), we have obtained the dark-bright soliton and semirational rogue-wave solutions for Eqs. (1).

We have observed the dark-bright one solitons with single-hump, double-hump, and breather-like structures, as shown in Figs. 1–3. Figs. 2 and 3 have shown two types of the breather-like one soliton. Figure 4 has shown the bound states between the breather and dark-bright soliton. Figures 5–7 have shown the different interactions between the double-peak breather and dark-bright solitons. In Figs. 8–11, we have seen that the rogue waves coexist and interact with dark-bright solitons. As shown in Fig. 9, the single-hump soliton maybe convert into the double-hump soliton after such interaction. Figure 11 has demonstrated that the single-peak and double-peak rogue waves coexist and interact with the dark-bright breather-like solitons. Figure 12 has shown the coexistence of the solitons with different velocities and rogue waves. Moreover, we use numerical simulations to study the stabilities of the dark-bright solitons and semirational rogue waves in a short propagation distance z, as shown in Figs. 13–16.

In nonlinear fiber optics, local wave phenomena have been confirmed in some experiments [9,10,38–41]. For instance, some interactions between the optical spatial solitons have been demonstrated through the experiments [38]. Breathers and rogue waves for the scalar NLS equation have been observed in the optical fiber experiments [9,10]. For vector solitons, the experiments of the incoherently coupled photorefractive spatial-soliton pairs (including the dark-bright solitons) have been shown [39]. Bright-dark soliton pairs with the orthogonal polarization have been generated in a passively mode-locked fiber laser with a large-angle tilted fiber grating [40]. Optical vector solitons with double-hump structures in optical Kerr media have been experimentally observed [41]. Vector dark rogue waves have also been investigated experimentally using standard fiber telecom equipment [42]. For the ultrashort pulses in the subpicosecond or femtosecond regime, setups proposed in Refs. [9,10,38–42] have given some possible experimental conditions about the observation of vector semirational rogue waves and interactions between breathers and dark-bright solitons. Therefore, we expect that the results in this paper may be useful for gaining further knowledge of solitons, breathers, and rogue waves.

ACKNOWLEDGMENTS

This work has been supported by the National Natural Science Foundation of China under Grants No. 11772017, No. 11272023, and No. 11471050, by the Fund of State Key Laboratory of Information Photonics and Optical Communications (Beijing University of Posts and Telecommunications), China (IPOC: 2017ZZ05), by the Fundamental Research Funds for the Central Universities of China under Grant No. 2011BUPTYB02, and by the Beijing University of Posts and Telecommunications Excellent Ph.D. Students Foundation (No. CX2017301).

APPENDIX: DERIVATION OF THE VECTOR SOLUTIONS OF LAX PAIR (2)

To obtain the vector solutions of Lax pair (2) under seed solutions (5), we need to consider the new vector eigenfunction

$$\hat{\Psi} = G^{-1}\Psi, \tag{A1}$$

with

$$G = \begin{pmatrix} 1 & 0 & 0 & 0 & 0 \\ 0 & \exp\left[i\vartheta + \frac{i}{2\epsilon}\left(kt - \frac{\omega}{4\epsilon}z\right)\right] & 0 & 0 & 0 \\ 0 & 0 & \exp\left[-i\vartheta - \frac{i}{2\epsilon}\left(kt - \frac{\omega}{4\epsilon}z\right)\right] & 0 & 0 \\ 0 & 0 & 0 & 1 & 0 \\ 0 & 0 & 0 & 0 & 1 \end{pmatrix}. \tag{A2}$$

Then Lax pair (2) can be rewritten as

$$\hat{\Psi}_t = \hat{U}(\lambda)\hat{\Psi}, \quad \hat{\Psi}_z = \hat{V}(\lambda)\hat{\Psi}, \tag{A3}$$

where

$$\hat{U}(\lambda)=\frac{i}{6\epsilon}\begin{pmatrix}-2\lambda & 3ic & 3ic & 0 & 0\\ -3ic & -K+\lambda & 0 & 0 & 0\\ -3ic & 0 & K+\lambda & 0 & 0\\ 0 & 0 & 0 & \lambda & 0\\ 0 & 0 & 0 & 0 & \lambda\end{pmatrix}, \tag{A4a}$$

$$\hat{V}(\lambda)=\frac{i\lambda}{2}\hat{U}^2(\lambda)-\frac{3+36c^2-K^2-6\lambda^2}{36\epsilon}\hat{U}(\lambda)+\frac{i\lambda(3\lambda^2+18c^2+K^2)}{108\epsilon^2}I_5+\frac{iK^2\lambda}{72\epsilon^2}A, \tag{A4b}$$

with

$$A=\begin{pmatrix}0 & 0 & 0 & 0 & 0\\ 0 & 0 & 0 & 0 & 0\\ 0 & 0 & 0 & 0 & 0\\ 0 & 0 & 0 & 1 & 0\\ 0 & 0 & 0 & 0 & 1\end{pmatrix},\quad K=1+3k.$$

Consequently, we can obtain the vector solutions of Lax pair (2) as

$$(v_1,v_2,v_3,v_4,v_5)^T=G\exp[\hat{U}(\lambda_1)t+\hat{V}(\lambda_1)z]Z_0, \tag{A5}$$

where Z_0 is a constant five-dimensional column vector. Without loss of generality, we set $Z_0=(1,\Gamma_1,\Gamma_2,\Gamma_3,\Gamma_4)^T$, where Γ_1, Γ_2, Γ_3, and Γ_4 are the complex constants.

We know that if $\hat{U}$ and $\hat{V}$ are similar to the diagonal matrix, $(v_1,v_2,v_3,v_4,v_5)^T$ is a linear combination of exponential vector functions of z and t, and q_1 and q_2 are exponential forms. If $\hat{U}$ and $\hat{V}$ are similar to the Jordan matrix, $(v_1,v_2,v_3,v_4,v_5)^T$ is a combination of exponential and polynomial vector functions of z and t, and q_1 and q_2 are semirational forms. Therefore, we focus on the matrix $-6i\epsilon\hat{U}(\lambda_1)$ and its characteristic polynomial

$$\det[m+6i\epsilon\hat{U}(\lambda_1)]=\big[m^3-\big(3\lambda_1^2+18c^2+K^2\big)m+2\lambda_1\big(\lambda_1^2+9c^2-K^2\big)\big](m-\lambda_1)^2.$$

It is noted that the equation $\det[m+6i\epsilon\hat{U}(\lambda_1)]=0$ has two known roots $m_4=m_5=\lambda_1$. To investigate whether $\hat{U}$ can be diagonalized, we consider the three roots m_1, m_2, and m_3 of the cubic equation

$$m^3-\big(3\lambda_1^2+18c^2+K^2\big)m+2\lambda_1\big(\lambda_1^2+9c^2-K^2\big)=0, \tag{A6}$$

Each solution m_l ($l=1,2,3$) depends on λ_1, c, and k.

There will be three cases of the roots for Eq. (A6), i.e., (i) the three roots are not equal to each other; (ii) there are a single root and a double root; (iii) there is a triple root. Since the seed solution q_{1s} is in nonzero background, similar to the scalar Sasa-Satsuma equation [33], we require spectral parameter $\lambda_1^2\notin\mathbb{R}$. Thus, case (iii) cannot be satisfied, and we only discuss two different cases in the following.

Case (i): m_1, m_2, and m_3 are not equal to each other

Under this case, $\hat{U}$ can be diagonalized. Setting the transformation matrix

$$T=\begin{pmatrix}1 & 1 & 1 & 0 & 0\\ \frac{-3ic}{m_1+K-\lambda_1} & \frac{-3ic}{m_2+K-\lambda_1} & \frac{-3ic}{m_3+K-\lambda_1} & 0 & 0\\ \frac{-3ic}{m_1-K-\lambda_1} & \frac{-3ic}{m_2-K-\lambda_1} & \frac{-3ic}{m_3-K-\lambda_1} & 0 & 0\\ 0 & 0 & 0 & 1 & 0\\ 0 & 0 & 0 & 0 & 1\end{pmatrix}, \tag{A7}$$

we have

$$T^{-1}\hat{U}(\lambda_1)T=\frac{i}{6\epsilon}\begin{pmatrix}m_1 & 0 & 0 & 0 & 0\\ 0 & m_2 & 0 & 0 & 0\\ 0 & 0 & m_3 & 0 & 0\\ 0 & 0 & 0 & \lambda_1 & 0\\ 0 & 0 & 0 & 0 & \lambda_1\end{pmatrix}, \tag{A8}$$

where

$$m_1=-\frac{\sqrt{\rho}(\varrho+\varrho^{-1})}{6}-\frac{i\sqrt{3\rho}(\varrho+\varrho^{-1})}{6}, \tag{A9a}$$

$$m_2=-\frac{\sqrt{\rho}(\varrho+\varrho^{-1})}{6}+\frac{i\sqrt{3\rho}(\varrho+\varrho^{-1})}{6}, \tag{A9b}$$

$$m_3=\frac{\sqrt{\rho}(\varrho+\varrho^{-1})}{3}, \tag{A9c}$$

with

$$\rho=3\big(3\lambda_1^2+18c^2+K^2\big),$$

$$\chi=\frac{-27\lambda_1\big(\lambda_1^2+9c^2-K^2\big)}{(\sqrt{\rho})^3},$$

$$\varrho=\sqrt[3]{\chi+\sqrt{\chi^2-1}}.$$

Via Eq. (A4b), $\hat{V}(\lambda_1)$ can also be reduced to a diagonal matrix by $T^{-1}\hat{V}(\lambda_1)T$. Then based on Eq. (A5), we derive

$$v_1=e^{i\xi_1}+\Gamma_1e^{i\xi_2}+\Gamma_2e^{i\xi_3}, \tag{A10a}$$

$$v_2=\exp\left[i\vartheta+\frac{i}{2\epsilon}\Big(kt-\frac{\omega}{4\epsilon}z\Big)\right]\times\big(r_{11}e^{i\xi_1}+\Gamma_1r_{12}e^{i\xi_2}+\Gamma_2r_{13}e^{i\xi_3}\big), \tag{A10b}$$

$$v_3=\exp\left[-i\vartheta-\frac{i}{2\epsilon}\Big(kt-\frac{\omega}{4\epsilon}z\Big)\right]\times\big(r_{21}e^{i\xi_1}+\Gamma_1r_{22}e^{i\xi_2}+\Gamma_2r_{23}e^{i\xi_3}\big), \tag{A10c}$$

$$v_4=\Gamma_3e^{i\xi_4},\quad v_5=\Gamma_4e^{i\xi_4}, \tag{A10d}$$

with

$$r_{jl} = \frac{-3ic}{m_l - (-1)^j K - \lambda_1}, \quad \xi_l = \frac{1}{6\epsilon}(m_l t + n_l z), \tag{A11a}$$

$$n_l = -\frac{1}{36\epsilon}\big[3\lambda_1 m_l^2 + \big(3 + 36c^2 - K^2 - 6\lambda_1^2\big)m_l - 2\lambda_1\big(3\lambda_1^2 + 18c^2 + K^2\big)\big], \tag{A11b}$$

$$\xi_4 = \frac{1}{6\epsilon}\left[\lambda_1 t + \frac{3\lambda_1^3 - \lambda_1}{12\epsilon} z\right], \quad j = 1,2, \quad l = 1,2,3. \tag{A11c}$$

Substituting Eqs. (A10) into Eqs. (4), we obtain the dark-bright soliton solutions for Eqs. (1).

Case(ii): $m_1 = m_2 = -\frac{1}{2}m_3$

When $m_1 = m_2 = -\frac{1}{2}m_3$, $\hat{U}$ is similar to a Jordan matrix. Setting the transformation matrix

$$T = \begin{pmatrix} 1 & 0 & 1 & 0 & 0 \\ \frac{-3ic}{m_1+K-\lambda_1} & \frac{3i\mu c}{(m_1+K-\lambda_1)^2} & \frac{-3ic}{m_3+K-\lambda_1} & 0 & 0 \\ \frac{-3ic}{m_1-K-\lambda_1} & \frac{3i\mu c}{(m_1-K-\lambda_1)^2} & \frac{-3ic}{m_3-K-\lambda_1} & 0 & 0 \\ 0 & 0 & 0 & 1 & 0 \\ 0 & 0 & 0 & 0 & 1 \end{pmatrix}, \tag{A12}$$

we have

$$T^{-1}\hat{U}(\lambda_1)T = \frac{i}{6\epsilon}\begin{pmatrix} m_1 & \mu & 0 & 0 & 0 \\ 0 & m_1 & 0 & 0 & 0 \\ 0 & 0 & m_3 & 0 & 0 \\ 0 & 0 & 0 & \lambda_1 & 0 \\ 0 & 0 & 0 & 0 & \lambda_1 \end{pmatrix}, \tag{A13}$$

where μ is the complex constant and

$$m_1 = \frac{3\lambda_1\big(\lambda_1^2 + 9c^2 - K^2\big)}{3\lambda_1^2 + 18c^2 + K^2}, \tag{A14a}$$

$$m_3 = -\frac{6\lambda_1\big(\lambda_1^2 + 9c^2 - K^2\big)}{3\lambda_1^2 + 18c^2 + K^2}, \tag{A14b}$$

with

$$\lambda_1 = \pm\frac{i\sqrt{18c^2(9c^2 + 10K^2) - 4K^4 + 6c(9c^2 - 4K^2)^{3/2}}}{6K}. \tag{A15}$$

In this case, we assume $9c^2 - 4K^2 < 0$, which follows from the requirement of $\lambda_1^2 \notin \mathbb{R}$. Similarly, $\hat{V}(\lambda_1)$ can be also reduced to a Jordan matrix. Via Eq. (A5), we derive

$$v_1 = e^{i\xi_1} + \Gamma_1 p_1 e^{i\xi_1} + \Gamma_2 e^{i\xi_3}, \tag{A16a}$$

$$v_2 = \exp\left[i\vartheta + \frac{i}{2\epsilon}\Big(kt - \frac{\omega}{4\epsilon}z\Big)\right] \times \big(r_{11}e^{i\xi_1} + \Gamma_1 p_2 e^{i\xi_1} + \Gamma_2 r_{13} e^{i\xi_3}\big), \tag{A16b}$$

$$v_3 = \exp\left[-i\vartheta - \frac{i}{2\epsilon}\Big(kt - \frac{\omega}{4\epsilon}z\Big)\right] \times \big(r_{21}e^{i\xi_1} + \Gamma_1 p_3 e^{i\xi_1} + \Gamma_2 r_{23} e^{i\xi_3}\big), \tag{A16c}$$

$$v_4 = \Gamma_3 e^{i\xi_4}, \quad v_5 = \Gamma_4 e^{i\xi_4}, \tag{A16d}$$

with

$$p_1 = \frac{i\mu}{216\epsilon^2}\big[36\epsilon t + \big(6\lambda_1^2 - 6\lambda_1 m_1 - 36c^2 + K^2 - 3\big)z\big], \tag{A17a}$$

$$p_2 = \frac{c\mu\big[36\epsilon t + \big(6\lambda_1^2 - 6\lambda_1 m_1 - 36c^2 + K^2 - 3\big)z\big]}{72\epsilon^2(m_1 + K - \lambda_1)} + \frac{3ic\mu}{(m_1 + K - \lambda_1)^2}, \tag{A17b}$$

$$p_3 = \frac{c\mu\big[36\epsilon t + \big(6\lambda_1^2 - 6\lambda_1 m_1 - 36c^2 + K^2 - 3\big)z\big]}{72\epsilon^2(m_1 - K - \lambda_1)} + \frac{3ic\mu}{(m_1 - K - \lambda_1)^2}, \tag{A17c}$$

where ξ_τ and r_{jl} are defined in Eqs. (A11). Via Eqs. (4), we obtain the semirational rogue-wave solutions for Eqs. (1).

[1] G. P. Agrawal, *Nonlinear Fiber Optics* (Academic, New York, 2007).

[2] E. A. Kuznetsov, A. M. Rubenchik, and V. E. Zakharov, Phys. Rep. **142**, 103 (1986).

[3] F. Dalfovo, S. Giorgini, L. P. Pitaevskii, and S. Stringari, Rev. Mod. Phys. **71**, 463 (1999).

[4] A. Chabchoub, N. P. Hoffmann, and N. Akhmediev, Phys. Rev. Lett. **106**, 204502 (2011).

[5] B. A. Malomed, D. Mihalache, F. Wise, and L. Torner, J. Opt. B **7**, R53 (2005).

[6] Y. S. Kivshar and B. Luther-Davies, Phys. Rep. **298**, 81 (1998).

[7] N. Akhmediev and V. I. Korneev, Theor. Math. Phys. **69**, 1089 (1986).

[8] N. Akhmediev, A. Ankiewicz, and J. M. Soto-Crespo, Phys. Rev. E **80**, 026601 (2009).

[9] B. Kibler, J. Fatome, C. Finot, G. Millot, F. Dias, G. Genty, N. Akhmediev, and J. M. Dudely, Nat. Phys. **6**, 790 (2010).

[10] B. Kibler, J. Fatome, C. Finot, G. Millot, G. Genty, B. Wetzel, N. Akhmediev, F. Dias, and J. M. Dudely, Sci. Rep. **2**, 463 (2012).

[11] S. V. Manakov, Sov. Phys.-JETP **38**, 248 (1974).

[12] R. Radhakrishnan and K. Aravinthan, J. Phys. A **40**, 13023 (2007); A. P. Sheppard and Y. S. Kivshar, Phys. Rev. E **55**, 4773 (1997); T. Kanna, M. Lakshmanan, P. T. Dinda, and N. Akhmediev, *ibid.* **73**, 026604 (2006).

[13] F. Baronio, A. Degasperis, M. Conforti, and S. Wabnitz, Phys. Rev. Lett. **109**, 044102 (2012); F. Baronio, M. Conforti, A. Degasperis, S. Lombardo, M. Onorato, and S. Wabnitz, *ibid.* **113**, 034101 (2014).

[14] S. Chen, J. M. Soto-Crespo, and P. Grelu, Opt. Exp. **22**, 27632 (2014); S. Chen and D. Mihalache, J. Phys. A **48**, 215202 (2015).

[15] S. Chen, F. Baronio, J. M. Soto-Crespo, P. Grelu, and D. Mihalache, J. Phys. A **50**, 463001 (2017).

[16] Y. Kodama, J. Stat. Phys. **39**, 597 (1985); Y. Kodama and A. Hasegawa, IEEE J. Quantum Elect. **23**, 510 (1987).

[17] K. Porsezian and K. Nakkeeran, Phys. Rev. Lett. **76**, 3955 (1996); M. Gedalin, T. C. Scott, and Y. B. Band, *ibid.* **78**, 448 (1997).
[18] K. Porsezian, P. Shanmugha Sundaram, and A. Mahalingam, Phys. Rev. E **50**, 1543 (1994).
[19] K. Nakkeeran, K. Porsezian, P. S. Sundaram, and A. Mahalingam, Phys. Rev. Lett. **80**, 1425 (1998).
[20] Y. Jiang and B. Tian, J. Mod. Opt. **63**, 1087 (2016).
[21] L. C. Zhao, Z. Y. Yang, and L. Ling, J. Phys. Soc. Jpn. **83**, 104401 (2014).
[22] H. Q. Zhang, Y. Wang, and W. X. Ma, Chaos **27**, 073102 (2017).
[23] T. Xu and X. M. Xu, Phys. Rev. E **87**, 032913 (2013); J. P. Wu and X. G. Geng, Commun. Theor. Phys. **67**, 527 (2017); L. Liu, B. Tian. H. M. Yin, and Z. Du, Wave Motion **80**, 91 (2018).
[24] D. Mihalache, L. Torner, F. Moldoveanu, N.-C. Panoiu, and N. Truta, J. Phys. A **26**, L757 (1993).
[25] T. Xu, M. Li, and L. Li, Europhys. Lett. **109**, 30006 (2015).
[26] U. Bandelow and N. Akhmediev, Phys. Lett. A **376**, 1558 (2012).
[27] U. Bandelow and N. Akhmediev, Phys. Rev. E **86**, 026606 (2012); S. Chen, *ibid.* **88**, 023202 (2013).
[28] J. M. Soto-Crespo, N. Devine, N. P. Hoffmann, and N. Akhmediev, Phys. Rev. E **90**, 032902 (2014).
[29] L. Liu, B. Tian, H. P. Chai, and Y. Q. Yuan, Phys. Rev. E **95**, 032202 (2017).
[30] G. Mu and Z. Y. Qin, Nonlinear Anal. Real. **31**, 179 (2016).
[31] V. B. Matveev and M. A. Salle, *Darboux Transformations and Solitons* (Springer, Berlin, 1991).
[32] A. Degasperis and S. Lombardo, J. Phys. A **42**, 385206 (2009).
[33] O. C. Wright III, Chaos, Solitons Fract. **33**, 374 (2007).
[34] M. J. Ablowitz, D. J. Kaup, A. C. Newell, and H. Segur, Phys. Rev. Lett. **31**, 125 (1973).
[35] Y. Ohta, *Nonlinear and Modern Mathematical Physics: Proceedings of the First International Workshop*, edited by W. X. Ma, X. Hu, and Qingping Liu, AIP Conf Proc. No. 1212 (AIP, New York, 2010), p. 114.
[36] K. Porsezian and V. C. Kuriakose, *Optical Solitons: Theoretical and Experimental Challenges* (Springer, Berlin, 2003).
[37] N. Akhmediev and A. Ankiewicz, Chaos **10**, 600 (2000).
[38] G. I. Stegeman and M. Segev, Science **286**, 1518 (1999).
[39] Z. Chen, M. Segev, T. H. Coskun, and D. N. Christodoulides, Opt. Lett. **21**, 1436 (1996); Z. Chen, M. Segev, T. H. Coskun, D. N. Christodoulides, Y. S. Kivshar, and V. V. Afanasjev, *ibid.* **21**, 1821 (1996); Z. Chen, M. Segev, T. H. Coskun, D. N. Christodoulides, and Y. S. Kivshar, J. Opt. Soc. Am. B **14**, 3066 (1997).
[40] Z. Zhang, C. Mou, Z. Yan, Z. Sun, and L. Zhang, Appl. Phys. B **122**, 161 (2016).
[41] C. Cambournac, T. Sylvestre, H. Maillotte, B. Vanderlinden, P. Kockaert, Ph. Emplit, and M. Haelterman, Phys. Rev. Lett. **89**, 083901 (2002).
[42] B. Frisquet, B. Kibler, P. Morin, F. Baronio, M. Conforti, G. Millot, and S. Wabnitz, Sci. Rep. **6**, 20785 (2016); B. Frisquet, B. Kibler, J. Fatome, P. Morin, F. Baronio, M. Conforti, G. Millot, and S. Wabnitz, Phys. Rev. A **92**, 053854 (2015).